

COMPUTING HYPERBOLIC CHOREOGRAPHIES

HADRIEN MONTANELLI*

Abstract. An algorithm is presented for numerical computation of choreographies in spaces of constant negative curvature in a hyperbolic cotangent potential, extending the ideas given in a companion paper [10] for computing choreographies in the plane in a Newtonian potential and on a sphere in a cotangent potential. Following an idea of Diacu, Pérez-Chavela and Reyes Victoria [6], we use stereographic projection and study the problem in the Poincaré disk. Using approximation by trigonometric polynomials and optimization methods with exact gradient and exact Hessian matrix, we find new choreographies, hyperbolic analogues of the ones presented in [10]. The algorithm proceeds in two phases: first BFGS quasi-Newton iteration to get close to a solution, then Newton iteration for high accuracy.

Key words. choreographies, n -body problem, trigonometric interpolation, quasi-Newton methods, Newton's method

AMS subject classifications. 70F10, 70F15, 70H12

1. Introduction. There is a growing interest in the n -body problem in spaces of constant curvature [1, 2, 3, 4, 5, 6, 7, 8, 11]. Recently, using numerical methods, the author has found new periodic solutions in the positive curvature case [10] (i.e., on the sphere \mathbb{S}_R^2 of radius R). These are very special periodic configurations in which the bodies share a common orbit and are uniformly spread along it, the *spherical choreographies*. Curved versions of the *planar choreographies* found by Simó in the early 2000s [12], they can be computed to high accuracy using stereographic projection, trigonometric interpolation and optimization. We show in this paper how these ideas can be used to find choreographies in spaces of negative curvature $-1/R^2$, the *hyperbolic choreographies*. These are hyperbolic analogues of the planar and spherical choreographies and, as $R \rightarrow +\infty$, they converge to the planar ones at a rate proportional to $1/R^2$.

2. Hyperbolic choreographies. While there really is only one model of two-dimensional spherical geometry (the sphere \mathbb{S}_R^2 with the great-circle distance), there are several models of hyperbolic geometry, including the Beltrami-Klein disk, the Poincaré disk, the Poincaré half-plane and the Lorentz hyperboloid models, with appropriate geodesic distances. In this paper, we use the latter, for which the equations of the n -body problem were first derived in [7] for general n , and using stereographic projection, we reformulate the problem on the Poincaré disk, following [6]. Once on the disk, we use the techniques presented in [10].

To describe hyperbolic geometry, the Lorentz model uses the forward sheet of a two-sheeted hyperboloid, defined as

$$\mathbb{L}_R^2 = \{X = (x_1, x_2, x_3)^T \in \mathbb{R}^3, X \odot X = -R^2, x_3 > 0\}, \quad R > 0, \quad (2.1)$$

with Lorentz inner product

$$X \odot Y = x_1 y_1 + x_2 y_2 - x_3 y_3 \quad (2.2)$$

*Oxford University Mathematical Institute, Oxford OX2 6GG, UK. Supported by the European Research Council under the European Union's Seventh Framework Programme (FP7/2007–2013)/ERC grant agreement no. 291068. The views expressed in this article are not those of the ERC or the European Commission, and the European Union is not liable for any use that may be made of the information contained here.

and Lorentz distance

$$d(X, Y) = \sqrt{(X - Y) \odot (X - Y)} \quad (2.3)$$

for $X = (x_1, x_2, x_3)^T$ and $Y = (y_1, y_2, y_3)^T$ on \mathbb{L}_R^2 . A two-sheeted hyperboloid with $R = 1$ is shown in Figure 2.1. The geodesic distance between X and Y on \mathbb{L}_R^2 is

$$\hat{d}(X, Y) = R \operatorname{acosh}\left(-\frac{X \odot Y}{R^2}\right). \quad (2.4)$$

The forward sheet \mathbb{L}_R^2 together with the geodesic distance (2.4) is called the *Lorentz hyperboloid model*. Note that this model uses *extrinsic coordinates*: \mathbb{L}_R^2 is embedded in \mathbb{R}^3 , i.e., points on \mathbb{L}_R^2 are represented by Cartesian coordinates in \mathbb{R}^3 .

The n -body problem on \mathbb{L}_R^2 describes the motion of n bodies on \mathbb{L}_R^2 with Cartesian coordinates $X_j(t) \in \mathbb{R}^3$, $0 \leq j \leq n-1$, via the n coupled nonlinear ODEs

$$X_j''(t) - \sum_{\substack{i=0 \\ i \neq j}}^{n-1} \frac{R^3 X_i(t) + R(X_i(t) \odot X_j(t))X_j(t)}{[(X_i(t) \odot X_j(t))^2 - R^4]^{3/2}} - R^{-2}(X_j'(t) \odot X_j'(t))X_j(t) = 0, \quad 0 \leq j \leq n-1. \quad (2.5)$$

The potential associated with (2.5) is a hyperbolic cotangent potential. We are looking for *hyperbolic choreographies*, i.e., solutions $X_j(t)$ such that

$$X_j(t) = Q\left(t + \frac{2\pi j}{n}\right), \quad 0 \leq j \leq n-1, \quad (2.6)$$

for some 2π -periodic function $Q : [0, 2\pi] \rightarrow \mathbb{L}_R^2$. We can choose the period equal to 2π since if $Q(t)$ is a T -periodic of (2.5) on \mathbb{L}_R^2 then $\lambda^{-2/3}Q(\lambda t)$, $\lambda = T/(2\pi)$, is a 2π -periodic solution in $\mathbb{L}_{R'}^2$ with $R' = \lambda^{-2/3}R$. As in the plane and on the sphere, they correspond to minima of the action associated with (2.5), defined as the integral over one period of the kinetic minus potential energy,

$$A = \int_0^{2\pi} (K(t) - U(t))dt, \quad (2.7)$$

with kinetic energy

$$K(t) = \frac{1}{2} \sum_{j=0}^{n-1} X_j'(t) \odot X_j'(t) = \frac{1}{2} \sum_{j=0}^{n-1} Q'\left(t + \frac{2\pi j}{n}\right) \odot Q'\left(t + \frac{2\pi j}{n}\right) \quad (2.8)$$

and potential energy

$$U(t) = -\frac{1}{R} \sum_{j=0}^{n-1} \sum_{i=0}^{j-1} \coth \frac{\hat{d}(X_i(t), X_j(t))}{R}. \quad (2.9)$$

Using the trigonometric identity $\cot(\operatorname{acosh}(x)) = x/\sqrt{x^2 - 1}$, the potential energy can be rewritten

$$U(t) = \frac{1}{R} \sum_{j=0}^{n-1} \sum_{i=0}^{j-1} \frac{X_i(t) \cdot X_j(t)}{\sqrt{(X_i(t) \odot X_j(t))^2 - R^4}}. \quad (2.10)$$

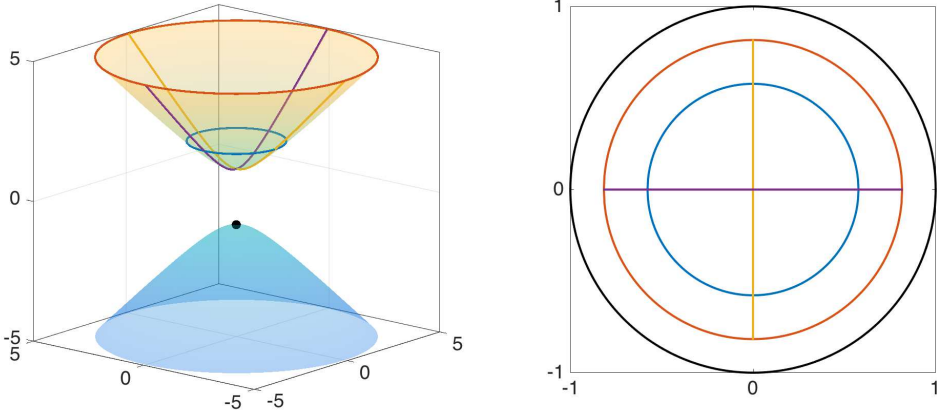


FIG. 2.1. On the left, a two-sheeted hyperboloid with $R = 1$. The space \mathbb{L}_R^2 corresponds to the forward sheet only. The blue and the red curves are sections $x_3 = 2$ and $x_3 = 5$ and correspond to circles of equations $x_1^2 + x_2^2 = -R^2 + 2^2$ and $x_1^2 + x_2^2 = -R^2 + 5^2$. The yellow and the purple curves are sections $x_1 = 0$ and $x_2 = 0$ and correspond to hyperbolas of equations $x_2^2 - x_3^2 = -R^2$ and $x_1^2 - x_3^2 = -R^2$. The north pole $(0, 0, -R)$ of the backward sheet is indicated by a black dot. On the right, the Poincaré disk $|z| < 1$, obtained using stereographic projection from the north pole of the backward sheet. The curves correspond to the projections of the curves of the same colour on the forward sheet. The black line, corresponding to $|z| = 1$, is the projection of the point at infinity.

Since the integral of (2.8) does not depend on j and the integral of (2.10) only depends on $i - j$, the action is given by

$$A = \frac{n}{2} \int_0^{2\pi} Q'(t) \odot Q'(t) dt - \frac{n}{2R} \sum_{j=1}^{n-1} \int_0^{2\pi} \frac{Q(t) \odot Q(t + \frac{2\pi j}{n})}{\sqrt{(Q(t) \odot Q(t + \frac{2\pi j}{n}))^2 - R^4}} dt. \quad (2.11)$$

We are also looking for *relative* hyperbolic choreographies,

$$X_j(t) = R_\omega(t) Q\left(t + \frac{2\pi j}{n}\right), \quad 0 \leq j \leq n-1, \quad R_\omega(t) = \begin{bmatrix} \cos(\omega t) & -\sin(\omega t) & 0 \\ \sin(\omega t) & \cos(\omega t) & 0 \\ 0 & 0 & 1 \end{bmatrix}, \quad (2.12)$$

i.e., choreographies rotating with angular velocity ω along the x_3 -axis. In this case, the kinetic part of (2.11) is

$$\frac{n}{2} \int_0^{2\pi} (R_\omega(t)Q'(t) + R'_\omega(t)Q(t)) \odot (R_\omega(t)Q'(t) + R'_\omega(t)Q(t)) dt. \quad (2.13)$$

Hyperbolic choreographies correspond to functions $Q(t)$ which minimize (2.11)–(2.13).

Now, let us reformulate this minimization problem on the Poincaré disk using stereographic projection. Points $X = (x_1, x_2, x_3)^T$ on \mathbb{L}_R^2 are mapped to points $z = P_R(X)$ on the Poincaré disk $\mathbb{D}_R^2 = \{z \in \mathbb{C}, |z| < R\}$ via

$$z = P_R(X) = \frac{Rx_1 + iRx_2}{R + x_3}. \quad (2.14)$$

The inverse mapping is given by

$$X = P_R^{-1}(z) = \frac{1}{R^2 - |z|^2} (2R^2 \operatorname{Re}(z), 2R^2 \operatorname{Im}(z), R^3 + R|z|^2)^T. \quad (2.15)$$

Note that (2.14) is a stereographic projection from the north pole $(0, 0, -R)$ of the backward sheet of the hyperboloid—see Figure 2.1 for an example of such a projection. The Lorentz distance (2.3) between two points on \mathbb{L}_R^2 is transformed into the distance $d(z, \xi)$ between their projections $z = P_R(X)$ and $\xi = P_R(Y)$ defined as

$$d(z, \xi) = \frac{2R^2 |z - \xi|}{\sqrt{(R^2 - |z|^2)(R^2 - |\xi|^2)}}, \quad (2.16)$$

and the geodesic distance (2.4) into

$$\hat{d}(z, \xi) = 2R \operatorname{asinh} \frac{d(z, \xi)}{2R}. \quad (2.17)$$

The Poincaré disk \mathbb{D}_R^2 together with the geodesic distance (2.17) is called the *Poincaré disk model*. This model uses *intrinsic coordinates* since points on \mathbb{D}_R^2 are represented by complex coordinates, i.e., \mathbb{D}_R^2 is not embedded in any higher dimensional space. Let $q(t) = P_R(Q(t))$ denote the projection of $Q(t) \in \mathbb{L}_R^2$ onto \mathbb{D}_R^2 , and

$$z_j(t) = P_R(X_j(t)) = P_R\left(Q\left(t + \frac{2\pi j}{n}\right)\right) = q\left(t + \frac{2\pi j}{n}\right), \quad 0 \leq j \leq n-1, \quad (2.18)$$

the projections of the n bodies. The kinetic part (2.13) of the action can be rewritten as

$$\frac{n}{2} \int_0^{2\pi} \left(\frac{2R^2 |q'(t) + i\omega q(t)|}{R^2 - |q(t)|^2} \right)^2 dt \quad (2.19)$$

with conformal factor $4R^4/(R^2 - |q(t)|^2)^2$. To derive the formula for the potential part of (2.11) in intrinsic coordinates, let us come back to the potential energy (2.10). On the Poincaré disk \mathbb{D}_R^2 , it is given by

$$U(t) = -\frac{1}{R} \sum_{j=0}^{n-1} \sum_{i=0}^{j-1} \coth \frac{\hat{d}(z_i(t), z_j(t))}{R} = -\frac{1}{R} \sum_{j=0}^{n-1} \sum_{i=0}^{j-1} \coth \left(2 \operatorname{asinh} \frac{d(z_i, z_j)}{2R} \right). \quad (2.20)$$

Using the trigonometric identity $\coth(2 \operatorname{asinh}(x/2)) = (x^2/2 + 1)/(x\sqrt{x^2/4 + 1})$ and integrating over one period, we find that the action is given by

$$A = \frac{n}{2} \int_0^{2\pi} \left(\frac{2R^2 |q'(t) + i\omega q(t)|}{R^2 - |q(t)|^2} \right)^2 dt + \frac{n}{2R} \sum_{j=1}^{n-1} \int_0^{2\pi} \frac{2R^2 + D_j(t)^2}{D_j(t) \sqrt{4R^2 + D_j(t)^2}} dt, \quad (2.21)$$

with $D_j(t) = d(q(t), q(t + \frac{2\pi j}{n}))$. Hyperbolic choreographies correspond to functions $q(t)$ which minimize (2.21).

3. Computing hyperbolic choreographies. Our method for computing hyperbolic choreographies is based on the algorithm presented in [10]—we summarize here quickly the key ideas behind this algorithm, and refer to [10] for details.

The algorithm uses trigonometric interpolation and numerical optimization of the action (2.21). The function $q(t)$ is represented by its trigonometric interpolant in the $\exp(ikt)$ basis. The optimization variables are the real and imaginary parts of its Fourier coefficients and the action is computed with the exponentially accurate trapezoidal rule [13]. Closed-form expressions for the gradient and the Hessian of the action with respect to the optimization variables can be derived and are used in the numerical optimization, which is carried out in two phases.

Phase 1. Quasi-Newton optimization methods. Numerical optimization methods with the exact gradient and based on approximations of the Hessian are employed with a small number of optimization variables. The accuracy of the solution at this stage is from one to five digits. This phase is computationally very cheap.

Phase 2. Newton's method. Once an approximation to a choreography has been computed via a quasi-Newton method, one can improve the accuracy to typically ten digits with a few steps of Newton's method with exact Hessian, and a larger number of optimization variables. This phase is computationally more expensive.

We use Chebfun [9], its extension to periodic problems [14] and MATLAB `fminunc` code for our computations. Once a choreography has been computed by our algorithm, we check that its Fourier coefficients decay to sufficiently small values, the gradient of the action (2.21) has small norm and that it is a solution of the equations of motion (2.5) projected onto the Poincaré disk. The latter were first derived in [6] and are given by

$$z_j''(t) = -\frac{2\bar{z}_j(t)z_j'^2(t)}{R^2 - |z_j(t)|^2} + \frac{4R}{\lambda_j(t)} \sum_{\substack{i=0 \\ i \neq j}}^{n-1} \frac{P_{j,i}(t)}{\Theta_{j,i}(t)^{3/2}}, \quad 0 \leq j \leq n-1, \quad (3.1)$$

where $\lambda_j(t) = 4R^4/(R^2 - |z_j(t)|^2)^2$ is the conformal factor introduced before, while $P_{j,i}(t)$ and $\Theta_{j,i}(t)$ are defined by

$$P_{j,i}(t) = [R^2 - |z_j(t)|^2][R^2 - |z_i(t)|^2]^2 [R^2 - \bar{z}_i(t)z_j(t)][z_i(t) - z_j(t)], \quad (3.2)$$

and

$$\Theta_{j,i}(t) = [2R^2z_j(t)\bar{z}_i(t) + 2R^2z_i(t)\bar{z}_j(t) - (|z_j(t)|^2 + R^2)(|z_i(t)|^2 + R^2)]^2 - [R^2 - |z_j(t)|^2]^2 [R^2 - |z_i(t)|^2]^2. \quad (3.3)$$

The first choreography that we present is the hyperbolic figure-eight of the three-body problem with $R = 1.5$, see Figure 3.1. Table 3.1 shows that, after 87 iterations of the first phase, the choreography satisfies (3.1) to six digits and after two iterations of the second phase it satisfies it to twelve digits. Figure 3.2 shows the Fourier coefficients of the solution, they decay to about 10^{-10} after the first phase and to about 10^{-16} after the second phase. We see in Table 3.1 that this choreography satisfies (3.1) to 12 digits of accuracy after the second phase.

Many choreographies can be found with our algorithm. We show in Figure 3.3 three hyperbolic choreographies of the five-body problem with $R = 1.2$. These are curved versions of the choreographies found by Simó in [12]. As shown in Table 3.2, they can be computed to high accuracy with a few hundred Fourier coefficients.

Relative choreographies can also be computed, see Figure 3.4. Again, a few hundred coefficients is enough to get about 10-digit accuracy.

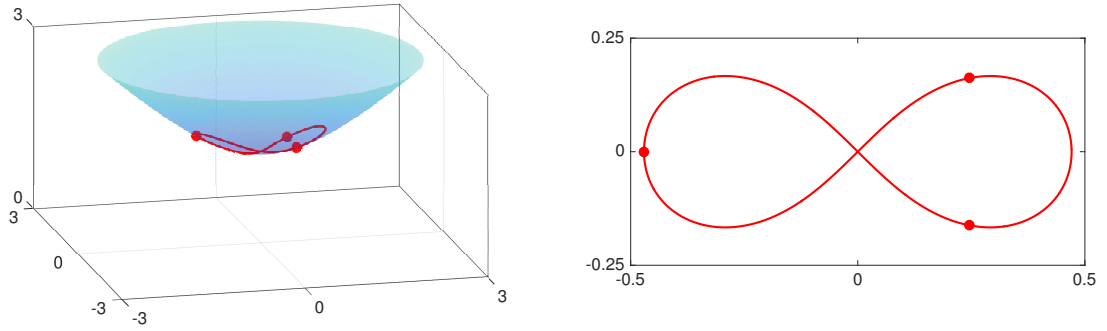


FIG. 3.1. *Hyperbolic figure-eight with $R = 1.5$ (left) and its projection on the Poincaré disk (right). The dots show the bodies at time $t = 0$. This choreography can be computed to about twelve digits of accuracy in less than 1.5 seconds on a 2.7 GHz Intel i7 machine.*

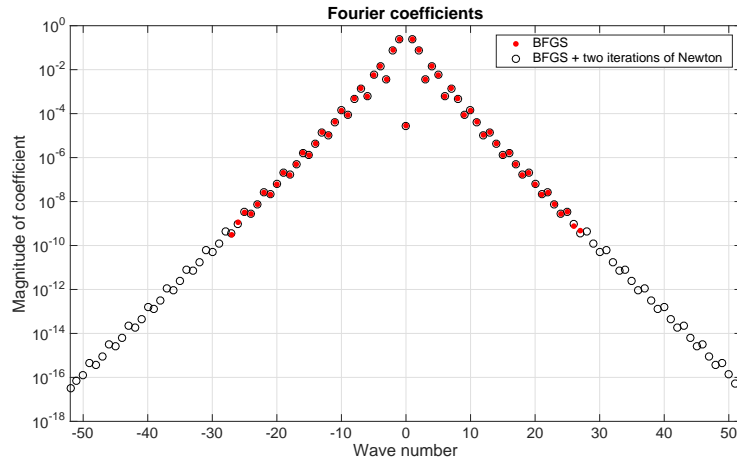


FIG. 3.2. *Absolute values of the Fourier coefficients of the hyperbolic figure-eight of Figure 3.1, obtained by BFGS (red dots) and BFGS followed by two steps of Newton's method (black circles).*

	Phase 1: BFGS	Phase 2: Newton
Action	27.840867421590943	27.840867421590929
Number of coefficients	55	105
Computer time (s)	0.7734	0.6427
Number of iterations	87	2
Relative 2-norm of the gradient	8.08e-08	3.87e-15
Smallest coefficient	4.75e-10	1.03e-16
Relative 2-norm of the residual	9.38e-07	3.54e-13

TABLE 3.1
Two-phase computation of the hyperbolic figure-eight of Figure 3.1.

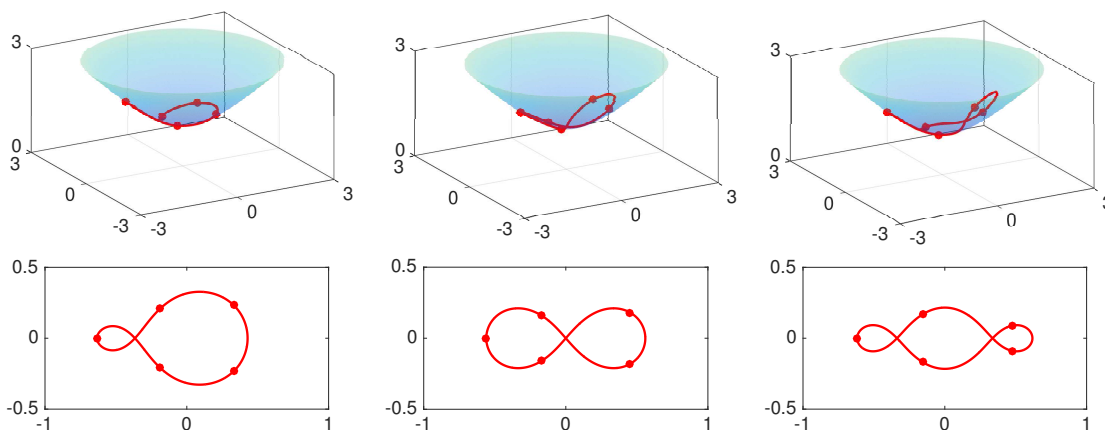


FIG. 3.3. *Hyperbolic choreographies with $R = 1.2$ (top) and their projections on the Poincaré disk (bottom). The dots show the bodies at time $t = 0$.*

	Phase 1	Phase 2	Phase 1	Phase 2	Phase 1	Phase 2
Action	88.8733	88.8733	90.6073	90.6073	96.2604	96.2604
Number of coefficients	75	305	55	155	65	245
Computer time (s)	2.52	17.54	0.75	3.02	1.03	10.88
Number of iterations	112	4	68	2	105	4
Relative 2-norm of the gradient	2.76e-08	5.82e-13	1.03e-07	8.30e-15	2.96e-09	9.89e-15
Smallest coefficient	1.55e-06	1.33e-17	1.13e-09	3.45e-18	3.85e-08	5.91e-18
Relative 2-norm of the residual	3.56e-03	3.54e-12	7.23e-06	3.57e-13	4.58e-03	2.03e-12

TABLE 3.2
Computation of the hyperbolic choreographies of Figure 3.3.

4. Limit of infinitely large R . In the limit $R \rightarrow \infty$, the Poincaré disk converges to the complex plane. The distances (2.16) and (2.17) converge to twice the absolute value and the action (2.13) converges to four times the action in the plane, since it involves squares of distances. As a consequence, twice the hyperbolic choreographies converge to the planar ones as $R \rightarrow \infty$, as shown in Figures 4.1 and 4.2. Tables 4.1 and 4.2 report the ∞ -norm of the difference between analogous hyperbolic and planar choreographies as R increases. The convergence appears to be at rate proportional to the absolute value of the curvature $1/R^2$.

5. Discussion. We have shown numerical evidence that choreographies also exist in spaces of constant negative curvature. As in the plane and on the sphere, they can be computed to high accuracy using trigonometric interpolation and minimization of the action.

REFERENCES

- [1] A. V. BORISOV, I. S. MAMAEV, AND A. A. KILIN, *Two-body problem on a sphere: reduction, stochasticity, periodic orbits*, Regul. Chaotic Dyn., 9 (2004), pp. 265–279.

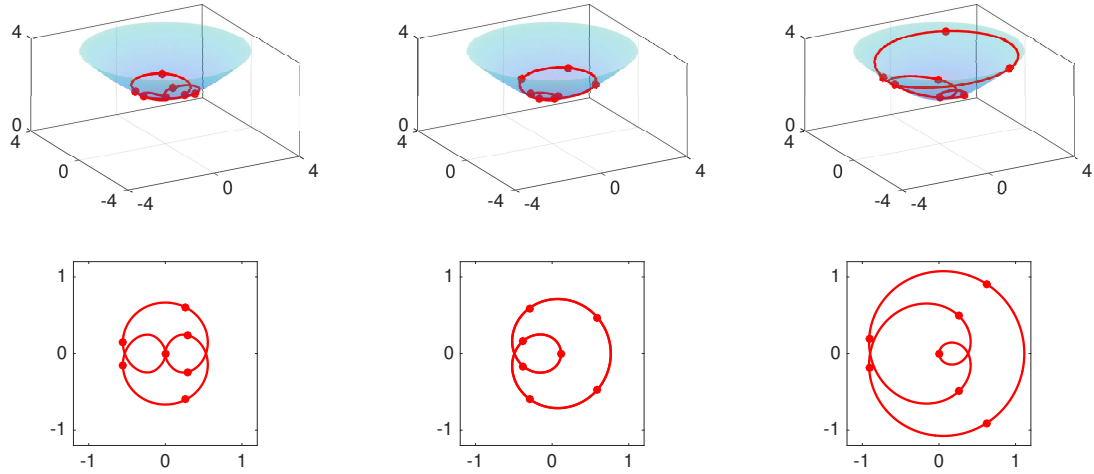


FIG. 3.4. First row: relative hyperbolic choreographies with $R = 2$ and angular velocities 2.8 (left), -2.9 (center) and 2.31 (right). Second row: their projections on the Poincaré disk. The dots show the bodies at time $t = 0$.

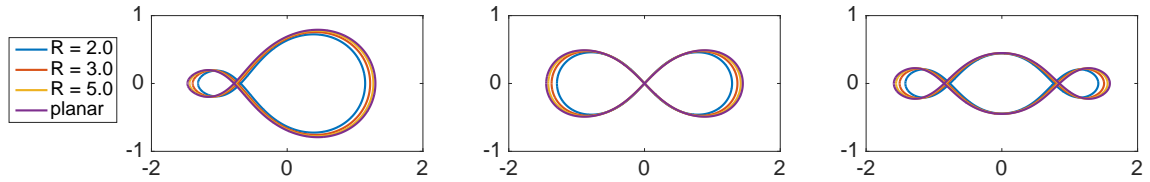


FIG. 4.1. Hyperbolic choreographies of Figure 3.3 (multiplied by a factor of 2) for different values of R . As R increases, the hyperbolic choreographies converge to the planar ones.

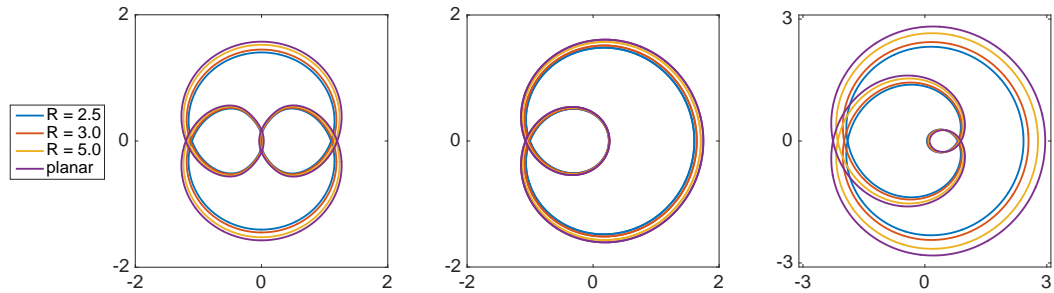


FIG. 4.2. Relative hyperbolic choreographies of Figure 3.4 (multiplied by a factor of 2) for different values of R . As R increases, the hyperbolic choreographies converge to the planar ones.

	$R = 2$	3	5	10	100	1000
Left	1.56e-01	7.74e-02	3.03e-02	7.87e-03	7.98e-05	7.99e-07
Middle	1.59e-01	7.97e-02	3.09e-02	7.98e-03	8.07e-05	8.14e-07
Right	1.70e-01	8.54e-02	3.31e-02	8.55e-03	8.65e-05	8.65e-07

TABLE 4.1

Convergence of the hyperbolic choreographies to the planar ones in Figure 4.1.

	$R = 2.5$	3	5	10	100	1000
Left	1.70e-01	1.25e-01	4.93e-02	1.28e-02	1.30e-04	1.31e-06
Middle	1.43e-01	1.05e-01	4.07e-02	1.05e-02	1.07e-04	1.09e-06
Right	5.34e-01	4.11e-01	1.77e-01	4.87e-02	5.03e-04	5.04e-06

TABLE 4.2

Convergence of the relative hyperbolic choreographies to the planar ones in Figure 4.2.

- [2] J. F. CARIÑENA AND M. F. RAÑADA, *Central potential on spaces of constant curvature: the Kepler problem on the two-dimensional sphere \mathbb{S}^2 and the hyperbolic plane \mathbb{H}^2* , J. Math. Phys., 46 (2005), p. 052702.
- [3] F. DIACU, *Relative equilibria of the curved N -body problem*, Springer, New York, 2012.
- [4] F. DIACU, R. MARTÍNEZ, E. PÉREZ-CHAVALA, AND C. SIMÓ, *On the stability of tetrahedral relative equilibria in the positively curved 4-body problem*, Phys. D, 256-257 (2013), pp. 21–35.
- [5] F. DIACU AND E. PÉREZ-CHAVALA, *Homographic solutions of the curved 3-body problem*, J. Differential Equations, 250 (2011), pp. 340–366.
- [6] F. DIACU, E. PÉREZ-CHAVALA, AND J. G. REYES VICTORIA, *An intrinsic approach in the curved n -body problem. The negative curvature case*, J. Differential Equations, 252 (2012), pp. 4529–4562.
- [7] F. DIACU, E. PÉREZ-CHAVALA, AND M. SANTOPRETE, *The n -body problem in spaces of constant curvature. Part I: relative equilibria*, J. Nonlinear Sci., 22 (2012), pp. 247–266.
- [8] ———, *The n -body problem in spaces of constant curvature. Part II: singularities*, J. Nonlinear Sci., 22 (2012), pp. 267–275.
- [9] T. A. DRISCOLL, N. HALE, AND L. N. TREFETHEN, eds., *Chebfun Guide*, Pafnuty Publications, Oxford, 2014; see also www.chebfun.org.
- [10] H. MONTANELLI AND N. I. GUSHTEROV, *Computing planar and spherical choreographies*, SIAM J. Appl. Dyn. Syst., 15 (2016), pp. 235–256.
- [11] E. PÉREZ-CHAVELA AND J. G. REYES VICTORIA, *An intrinsic approach in the curved n -body problem. The positive curvature case*, Trans. Amer. Math. Soc., 364 (2012), pp. 3805–3827.
- [12] C. SIMÓ, *New families of solutions in N -body problems*, in Proceedings of the Third European Congress of Mathematics, Basel, 2001, Birkhäuser.
- [13] L. N. TREFETHEN AND J. A. C. WEIDEMAN, *The exponentially convergent trapezoidal rule*, SIAM Rev., 56 (2014), pp. 385–458.
- [14] G. B. WRIGHT, M. JAVED, H. MONTANELLI, AND L. N. TREFETHEN, *Extension of Chebfun to periodic functions*, SIAM J. Sci. Comp., 37 (2015), pp. C554–C573.